Photoelectron spectroscopy of $B_4O_4^-$: Dual 3c-4e π hyperbonds and rhombic 4c-4e o-bond in boron oxide clusters

Wen-Juan Tian, Li-Juan Zhao, Qiang Chen, Ting Ou, Hong-Guang Xu, Wei-Jun Zheng, Hua-Jin Zhai, and Si-Dian Li

Citation: The Journal of Chemical Physics **142**, 134305 (2015); doi: 10.1063/1.4916386
View online: http://dx.doi.org/10.1063/1.4916386
View Table of Contents: http://aip.scitation.org/toc/jcp/142/13
Published by the American Institute of Physics

Photoelectron spectroscopy of $B_4O_4^-$: Dual 3c-4e π hyperbonds and rhombic 4c-4e *o*-bond in boron oxide clusters

Wen-Juan Tian,[1,a)] Li-Juan Zhao,[2,3,a)] Qiang Chen,[1] Ting Ou,[1] Hong-Guang Xu,[2] Wei-Jun Zheng,[2,b)] Hua-Jin Zhai,[1,4,b)] and Si-Dian Li[1,b)]
[1]*Nanocluster Laboratory, Institute of Molecular Science, Shanxi University, Taiyuan 030006, China*
[2]*State Key Laboratory of Molecular Reaction Dynamics, Institute of Chemistry, Chinese Academy of Sciences, Beijing 100190, China*
[3]*University of Chinese Academy of Sciences, Beijing 100049, China*
[4]*State Key Laboratory of Quantum Optics and Quantum Optics Devices, Shanxi University, Taiyuan 030006, China*

(Received 21 January 2015; accepted 17 March 2015; published online 3 April 2015)

Gas-phase anion photoelectron spectroscopy (PES) is combined with global structural searches and electronic structure calculations at the hybrid Becke 3-parameter exchange functional and Lee-Yang-Parr correlation functional (B3LYP) and single-point coupled-cluster with single, double, and perturbative triple excitations (CCSD(T)) levels to probe the structural and electronic properties and chemical bonding of the $B_4O_4^{0/-}$ clusters. The measured PES spectra of $B_4O_4^-$ exhibit a major band with the adiabatic and vertical detachment energies (ADE and VDE) of 2.64 ± 0.10 and 2.81 ± 0.10 eV, respectively, as well as a weak peak with the ADE and VDE of 1.42 ± 0.08 and 1.48 ± 0.08 eV. The former band proves to correspond to the Y-shaped global minimum of C_s $B_4O_4^-$ ($^2A''$), with the calculated ADE/VDE of 2.57/2.84 eV at the CCSD(T) level, whereas the weak band is associated with the second lowest-energy, rhombic isomer of D_{2h} $B_4O_4^-$ ($^2B_{2g}$) with the predicted ADE/VDE of 1.43/1.49 eV. Both anion structures are planar, featuring a B atom or a B_2O_2 core bonded with terminal BO and/or BO_2 groups. The same Y-shaped and rhombic structures are also located for the B_4O_4 neutral cluster, albeit with a reversed energy order. Bonding analyses reveal dual three-center four-electron (3c-4e) π hyperbonds in the Y-shaped $B_4O_4^{0/-}$ clusters and a four-center four-electron (4c-4e) π bond, that is, the so-called *o*-bond in the rhombic $B_4O_4^{0/-}$ clusters. This work is the first experimental study on a molecular system with an *o*-bond. © *2015 AIP Publishing LLC*. [http://dx.doi.org/10.1063/1.4916386]

I. INTRODUCTION

Over the past decade, persistent experimental and computational effort has been devoted to the elucidation of the structural and electronic properties and chemical bonding of elemental boron clusters, a prototypical electron-deficient molecular system. A rich variety of novel cluster structures were discovered, such as the planar or quasi-planar boron clusters in a wide range of sizes ($B_n^{-/0}$, n = 3–25, 30, 35, 36),[1–21] the tubular boron rings,[12,22–28] and the double-chain boron nanoribbons.[29–32] A recent work[33] reported the discovery of all-boron fullerenes or borospherenes, B_{40} and B_{40}^-, which was followed closely by the theoretical prediction of metalloborospherenes: endohedral M@B_{40} (M = Ca, Sr) and exohedral M&B_{40} (M = Be, Mg).[34] Subsequently, an axially chiral borospherene B_{39}^- was also characterized.[35] The electron deficiency of boron underlies the unique structures and bonding of the boron clusters, which are governed entirely by aromaticity and antiaromaticity. Boron is also well known for its oxygen affinity. Upon oxidation of boron clusters, the boron oxide clusters[36–56] are anticipated to be even more electron-deficient, suggesting vast opportunities to explore novel molecular structures and exotic chemical bonding.

The boronyl (BO) group with a B≡O triple bond is isovalent to the cyano (CN) group, both of which are known as monovalent σ-radicals.[46–48,55] A variety of boron oxide clusters were studied in the past years, demonstrating that the BO group plays a key role in their structures and bonding. The ratio of B versus O represents a new parameter to alter and tune the properties of boron oxide clusters. However, current knowledge of the oxygen-rich B_nO_m clusters and those with equal content of boron and oxygen is limited. Our recent effort along this line led to the computational design of the boronyl boroxine, D_{3h} $B_3O_3(BO)_3$, a boron oxide analogue of benzene and boroxine.[57] In another computational work,[55] we studied the structural and bonding properties of a series of $B_3O_n^{-/0/+}$ (n = 2–4) clusters, and further uncovered the dual three-center four-electron (3c-4e) π hyperbonds and the rhombic four-center four-electron (4c-4e) π bond in boron oxide clusters, the latter being also called an *o*-bond.

In this contribution, we report a joint experimental and theoretical study on the $B_4O_4^{0/-}$ clusters using photoelectron spectroscopy (PES), global structural searches, and electronic structure calculations. The $B_4O_4^{0/-}$ clusters also have a B/O ratio of 1:1, similar to the boronyl boroxine.[57] The concerted results show that the B_4O_4 and $B_4O_4^-$ clusters adapt distinctly different global-minimum structures: Y-shaped C_s (**1**) for the anion and rhombic D_{2h} (**3**) for the neutral. The C_s structure features a B atom bonded terminally to one OBO

[a)]W.-J. Tian and L.-J. Zhao contributed equally to this work.
[b)]Author to whom correspondence should be addressed. Electronic addresses: zhengwj@iccas.ac.cn; hj.zhai@sxu.edu.cn; and lisidian@sxu.edu.cn.

(that is, BO_2) unit and two boronyl groups, whereas the D_{2h} structure has a B_2O_2 core with two terminal boronyl groups. Both the Y-shaped C_s (**1**) and rhombic D_{2h} (**2**) anion isomers are observed in the experiment, with the C_s structure being predominant. The neutral D_{2h} (**3**) and C_s (**4**) isomers are accessed upon photodetachment and very different electron affinities are observed: 1.42 ± 0.08 eV for D_{2h} versus 2.64 ± 0.10 eV for C_s. Chemical bonding analyses reveal the dual 3c-4e ω hyperbonds in C_s $B_4O_4^{0/-}$ structures and the rhombic 4c-4e *o*-bond in D_{2h} $B_4O_4^{0/-}$ species. To our knowledge, this work is the first experimental study on a gas-phase cluster with an *o*-bond.

II. EXPERIMENTAL AND THEORETICAL METHODS

A. Photoelectron spectroscopy

The experiment was carried out on a home-built PES apparatus, which consists of a laser vaporization cluster source, a time-of-flight (TOF) mass spectrometer, and a magnetic-bottle photoelectron spectrometer. The details of apparatus have been described elsewhere.[58] The $B_4O_4^-$ cluster anions were generated from a rotating and translating B_2O_3 disc target with the second harmonic of a nanosecond Nd:YAG laser (Continuum Surelite II-10). The typical laser power used for vaporization was about 10 mJ per pulse in this work. Helium carrier gas with ~4 atm backing pressure was used to cool down the formed clusters by expansion through a pulsed valve (General Valve Series 9). The $B_4O_4^-$ anions were selected using a mass gate, decelerated by a momentum decelerator, and photodetached with the beam of another Nd:YAG laser (Continuum Surelite II-10; 532, 355, and 266 nm). The photoelectrons produced were energy-analyzed using the magnetic-bottle photoelectron spectrometer. The PES data were calibrated using the spectra of Bi^-, Cs^-, Cu^-, and Au^- obtained under similar conditions. The resolution of the PES apparatus was about 40 meV at the electron kinetic energy of 1 eV.

B. Computational methods

The Coalescence Kick (CK)[59,60] and Minima Hopping (MH)[61–63] algorithms were used, independently, for the global-minimum structural searches, which were aided with manual structural constructions as well. About 2200 stationary points for $B_4O_4^-$, and the same number for B_4O_4, were probed in the CK and MH searches. The candidate low-lying structures were further optimized at the B3LYP/aug-cc-pVTZ level,[64] which is a popular, hybrid method involving the Becke 3-parameter exchange functional and the Lee-Yang-Parr correlation functional. Harmonic vibrational frequencies were analyzed at the same level to compute the zero-point energies and to verify that the reported structures are true minima on their potential energy surfaces.

Adiabatic and vertical detachment energies (ADEs and VDEs) were calculated at the B3LYP level for the ground-state transition and at time-dependent B3LYP (TD-B3LYP) level for the excited states.[65,66] The VDEs were also calculated at the outer valence Green's function (OVGF) level.[67–69] Furthermore, single-point coupled-cluster with single, double, and perturbative triple excitations (CCSD(T)) calculations[70–72] at the B3LYP geometries were done to benchmark the relative energies of the top structures for both the anion and the neutral and to refine the ADEs and VDEs. Adaptive natural density partitioning (AdNDP)[73] and canonical molecular orbital (CMO) analyses were performed to elucidate the bonding patterns. Natural bond orbital (NBO) analysis was carried out to get the natural atomic charges and the Wiberg bond indices.[74] The AdNDP calculations were performed using the AdNDP program and all other calculations were performed using the Gaussian 09 package.[75]

III. EXPERIMENTAL RESULTS

The PES spectra of the $B_4O_4^-$ anion cluster were recorded at the 532 nm (2.331 eV), 355 nm (3.496 eV), and 266 nm (4.661 eV) photon energies, as depicted in Fig. 1. The 266 nm spectrum (Fig. 1(c)) reveals a low binding energy feature X′ and a predominant, broad band X, which are centered at the VDEs of 1.48 ± 0.08 and ~2.8 eV, respectively. Band X is much stronger than band X′. As was recently done for B_{40}^- (Ref. 33), the X′/X ratio hints that these may originate from different isomeric species in the $B_4O_4^-$ anion beam.

The X′ band is better defined in the 532 nm (Fig. 1(a)) and 355 nm (Fig. 1(b)) spectra. It is resolved into a major, sharp peak at 1.48 eV and a broad shoulder in the regime of 1.6–2.0 eV, where the latter is likely due to unresolved vibrational structures. A tentative vibrational spacing of 0.12 eV (~950 cm^{-1}) is estimated for band X′. The broad band X is also better resolved at 355 nm with a VDE of 2.81 ± 0.10 eV (Fig. 1(b)), which exhibits four peaks centered at 2.64, 2.81, 2.94, and 3.05 eV, respectively, likely due to partially resolved

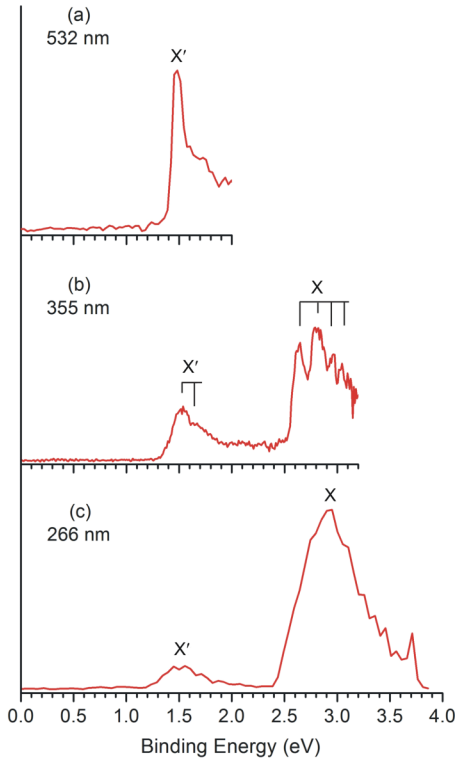

FIG. 1. Photoelectron spectra of the $B_4O_4^-$ anion cluster at (a) 532 nm, (b) 355 nm, and (c) 266 nm. The vertical lines represent the resolved vibrational structures.

vibrational progressions. Two vibrational modes are tentatively assigned: 0.17 eV (~1350 cm^{-1}) and 0.12 eV (~950 cm^{-1}). The ground-state ADEs were evaluated from the well-defined onset of band X′ and the first vibational peak of band X to be 1.42 ± 0.08 and 2.64 ± 0.10 eV, respectively, which also represent the electron affinities of the corresponding neutral species. All the experimental ADEs and VDEs are listed in Table I.

IV. THEORETICAL RESULTS

Global-minimum searches using the CK and MH algorithms allow the identification of the low-lying isomers for $B_4O_4^{0/-}$, whose optimized structures at the B3LYP/aug-cc-pVTZ level are shown in the supplementary material (Figs. S1 and S2),[76] along with their relative energies. The relative energies for top structures within 15 kcal/mol are further refined at the single-point CCSD(T) level. It appears that the global minima for both the anion and the neutral are well-defined: C_s $B_4O_4^-$ (**1**, $^2A''$) and D_{2h} B_4O_4 (**3**, ^1A_g) (Fig. 2). Their nearest isomeric structures, D_{2h} $B_4O_4^-$ (**2**, $^2B_{2g}$) and C_s B_4O_4 (**4**, $^1A'$), lie at 8.1 and 18.3 kcal/mol above the global minima, respectively, at the CCSD(T) level. All B and O atoms are labeled numerically in Figs. 2(a) and 2(b). Notably, the two anion structures **1** and **2** closely resemble those of the neutral (**3** and **4**), except that the energy order reverses from anion to neutral.

The calculated bond distances at the B3LYP level are shown in Fig. 2. The majority of the formal bond orders are readily assigned as follows. First, all three terminal BO bonds in Y-shaped **1**/**4** and two terminal BO bonds in rhombic **2**/**3** are typical B≡O triple bonds, with short distances (1.20–1.23 Å). Second, all BB bonds exhibit the distances of 1.64–1.69 Å and are assigned roughly as B—B single bonds.[77,78] Third, on the basis of chemical intuition, the B4—O8 bond in **1** (1.46 Å) and that in its corresponding anion **4** (1.36 Å) are roughly assigned as B—O single bond, as are all BO bonds within the rhombic rings in **2**/**3** (1.40–1.42 Å). The only tricky part concerns the B1—O8 bond in **1** (1.29 Å) and the corresponding bond in **4** (1.33 Å). These may be best described as B=O double bonds,[79] which will be discussed below in Sec. VI.

We would like to note the discernible shrink of the BB distances from neutral to anion, by ~0.05 Å from **4** to **1** and ~0.04 Å from **3** to **2**. This is consistent with the distribution of the extra electron in the **1** and **2** anions, which is shared by the BB bonds, effectively increasing the bond order by 0.25 for each BB bond. In addition, the B4—O8 distance expands (by ~0.1 Å) from neutral **4** and anion **1**, indicating substantial intramolecular Coulomb repulsion in the anion.

V. COMPARISON BETWEEN EXPERIMENT AND THEORY

The PES spectra of the $B_4O_4^-$ cluster are simple (Fig. 1), yet they provide definitive electronic structure information. They also hint the coexistence of two isomers in the $B_4O_4^-$ cluster beam (see Sec. III). The experimental ADEs and VDEs are compared with theoretical data at the B3LYP, OVGF, and single-point CCSD(T) levels in Table I. Obviously, the combination of structures **1** and **2** is in excellent agreement with the experimental data.

The ground-state ADE/VDE for the Y-shaped structure **1** is calculated to be 2.76/3.04 eV at the B3LYP level. These values are roughly in line with the experimental measurement of 2.64/2.81 eV for band X, albeit with the errors of 0.1–0.2 eV. The next detachment channel for **1** is the first triplet neutral state, $^3A''$, with a calculated VDE of 6.55 eV, which is beyond the range of the measured spectra. Interestingly, the rhombic isomer **2** produces a ground-state ADE/VDE of 1.81/1.91 eV at the B3LYP level, which corresponds to experimental band X′ (1.42/1.48 eV) with slightly larger errors. The second predicted channel for **2** is 6.67 eV, again beyond the photon energy range of the experiment.

To further ensure the PES assignments, we have also calculated the VDEs using the OVGF method. The calculated VDEs for structures **1** and **2** are 2.86 and 1.48 eV, respectively, which are in perfect agreement with the experimental values (2.81 and 1.48 eV). The OVGF results are markedly improved with respective to B3LYP, suggesting that OVGF performs much better for the current system. As a final benchmark, the single-point CCSD(T) calculations result in the ground-state VDEs of 2.84 and 1.49 eV for **1** and **2**, respectively, which are nearly identical to those at the OVGF level, again in perfect agreement with the experimental measurements. The ADEs for **1** and **2** at CCSD(T), 2.57/1.43 eV, are also in very good agreement with experiment (2.64/1.42 eV), with errors of less than 0.1 eV.

The tentative vibrational spacings in the PES spectra, ~950 cm^{-1} for X′ and ~950 and ~1350 cm^{-1} for X (Fig. 1), are assigned to the B—B stretching in **3** (947 cm^{-1} at B3LYP) and

TABLE I. Experimental ADEs and VDEs (in eV) from the photoelectron spectra of $B_4O_4^-$, as compared to those calculated at the B3LYP/aug-cc-pVTZ, OVGF, and single-point CCSD(T)//B3LYP/aug-cc-pVTZ levels.

			Expt.		B3LYP		OVGF	CCSD(T)	
Species	Feature	Final state	ADE[a,b]	VDE	ADE[b]	VDE	VDE	ADE[b]	VDE
$B_4O_4^-$ (**1**, $^2A''$)	X	$^1A'$	*2.64*[c]	2.81[c]	*2.76*	3.04	2.86	*2.57*	2.84
		$^3A''$				6.55	7.59		7.10
$B_4O_4^-$ (**2**, $^2B_{2g}$)	X′	^1A_g	*1.42*[d]	1.48[d]	*1.81*	1.91	1.48	*1.43*	1.49
		$^3B_{1u}$				6.67	7.37		7.14

[a]Electron affinity of the corresponding neutral cluster.
[b]All experimental and theoretical ADEs are shown in *italic*.
[c]Estimated experimental uncertainties: ±0.10 eV.
[d]Estimated experimental uncertainties: ±0.08 eV.

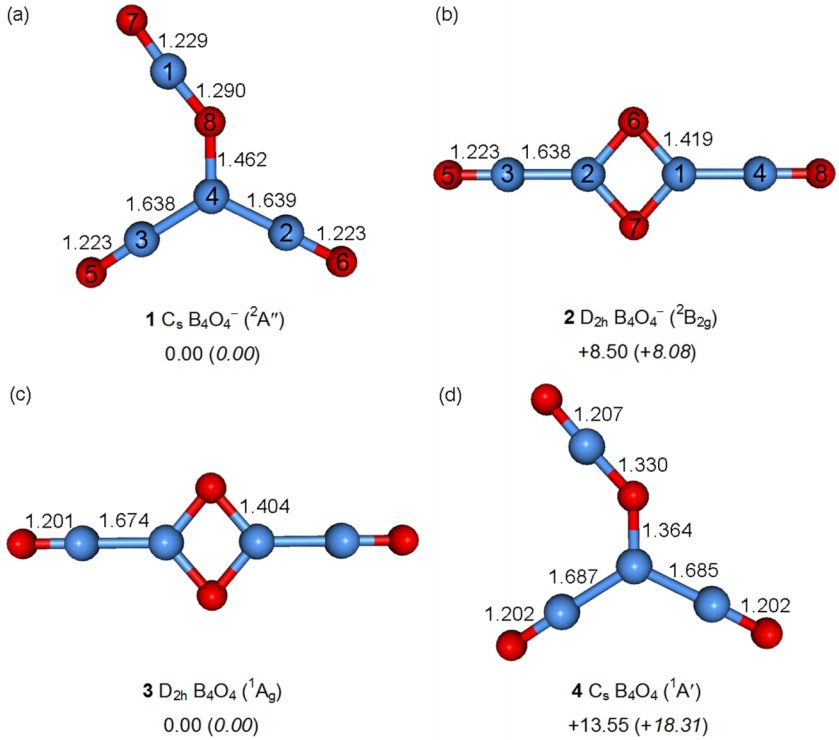

FIG. 2. Optimized global-minimum structures of $B_4O_4^{-/0}$ (**1** and **3**) and their low-lying isomers (**2** and **4**) at the B3LYP/aug-cc-pVTZ level. Relative energies (in kcal/mol) are shown at the B3LYP/aug-cc-pVTZ and CCSD(T)//B3LYP/aug-cc-pVTZ (in *italic*) levels. Bond distances (in Å) are labeled. All B and O atoms are labeled numerically in **1** and **2**. The B atom is in blue and O is in red.

the B—B and B4—O8 stretchings in **4** (930/943 and 1370 cm^{-1} at B3LYP), respectively. The predicted BB stretchings in **4** have a slight splitting due to symmetry reason. The above assignments of the vibrational modes are consistent with the nature of the frontier CMOs, where the extra electrons in the **1** and **2** anions are primarily located on the BBB or BB bonds (Fig. S3).[76] In short, the concerted B3LYP, OVGF, and single-point CCSD(T) data are in line with the experiment, lending considerable credence to the identified global minima and low-lying isomers for $B_4O_4^-$ and B_4O_4 (Fig. 2).

VI. DISCUSSION

A. Global-minimum structures

Two isomeric structures, the Y-shaped **1** (C_s, $^2A''$) and the rhombic **2** (D_{2h}, $^2B_{2g}$), coexist in the $B_4O_4^-$ anion beam, which are jointly responsible for the experimental PES spectra. Similar two structures (**3** and **4**) are identified as the global minimum and the second lowest in energy for the neutral cluster, except that the energy order reverses from anion to neutral. Thus, one extra electron makes a difference in terms of structure and bonding for such electron-deficient systems.

A key factor that governs the global-minimum structures of **1** (Y-shaped) for $B_4O_4^-$ versus **3** (rhombic) for B_4O_4 is the nature of the frontier CMOs. The extra electron in **1** occupies a delocalized, completely bonding 3c-1e BBB π CMO (Fig. S3),[76] which corresponds to the experimental band X with a VDE of ~2.8 eV. In contrast, the extra electron in **2** is largely fragmented over the two B_2 units with formal antibonding character between them, which has a substantially lower experimental VDE of ~1.5 eV (band X′). Thus, the extra electron gains an enhanced stabilization of ~1.3 eV for the Y-shaped isomer with respective to the rhombic one. This makes structure **1** the global minimum for the $B_4O_4^-$ anion, although structure **3** is the global minimum for the B_4O_4 neutral (Fig. 2). The NBO charge distribution in **1**–**4** (Fig. S4)[76] is generally in line with the nature of singly occupied molecular orbital (SOMO) of the anions. Alternatively, the stability of rhombic **3** neutral species may be understood via its large energy gap between its highest occupied and lowest unoccupied molecular orbitals (HOMOs and LUMOs), which amounts to ~5.6 eV at the CCSD(T) level (Table I), suggesting a remarkably robust neutral cluster. For comparison, the HOMO-LUMO gap is substantially smaller for the Y-shaped isomer **4** (~4.3 eV at CCSD(T)).

Interestingly, the Y-shaped C_s (**1**) and rhombic D_{2h} (**2**) $B_4O_4^-$ clusters show very different reorganization energies (ROEs). The ROE for a molecular species is defined as the difference between the ground-state ADE and VDE, which characterizes the anion-to-neutral structural changes upon electron detachment. The calculated ROEs amount to 0.27 and 0.06 eV for **1** and **2**, respectively, at the single-point CCSD(T) level (Table I). These are in good agreement with the experimental measurements: 0.17 eV for band X versus 0.06 eV for band X′. The ROEs suggest that the C_s $B_4O_4^-$ cluster is relatively floppy, whereas the D_{2h} $B_4O_4^-$ cluster is rather rigid, which are consistent with their geometries, providing further support for our structural assignments.

We would like to comment here that the relative ratio of rhombic isomer **2** versus Y-shaped isomer **1** in the experimental $B_4O_4^-$ anion beam (X′ versus X; Fig. 1) appears to be substantially greater than the Boltzmann distribution. With a relative energy of ~8 kcal/mol (Fig. 2), the intensity of isomer **2** is expected to be negligible thermodynamically. We attribute this behavior to the kinetic reason: the neutral global minimum **3** (rhombic) is far more stable than isomer **4** (Y-shaped), where the former readily produces anion isomer **2** upon electron

attachment in the laser plasma and the supersonic expansion. Once anion isomer **2** is formed, its conversion to the global minimum **1** would be difficult due to a large barrier between structures **1** and **2**. A similar case was reported in a prior study on the bare B_7^- cluster,[4] for which an *elongated* isomer about 8 kcal/mol above the *circular* global minimum was also observed to coexist in the cluster beam.

B. The Y-shaped C_s structures 1 and 4: Dual 3c-4e π hyperbonds

The terminal OBO unit is a key structural block in boron oxide clusters, such as **1** and **4** (Fig. 2). In structure **1**, the OBO block possesses BO distances of 1.23 and 1.29 Å, which is asymmetric. In **4**, the BO distances associated to the OBO block are even more asymmetric: 1.21 versus 1.33 Å. The shorter BO distances (1.23 Å in **1** and 1.21 Å in **4**) are typical for a B≡O triple bond, whereas the longer ones are comparable to or slightly greater than a B=O double bond (~1.28 Å). The latest recommended covalent radii for elements[79] put the upper limit of the B≡O, B=O, and B—O bonds to be 1.26, 1.35, and 1.48 Å, respectively. Thus, simply based on the bond distances, the BO bonds within the OBO block in **1** and **4** may be best assigned as B≡O and B=O bonds.

Chemical bonding analysis supports the above assignments. Figure 3(a) depicts the AdNDP bonding pattern for **1**. As an extension of the NBO analysis, AdNDP represents the bonding of a molecule in terms of *n*-center two-electron (*n*c-2e) bonds, with *n* ranging from one to the total number of atoms in the system. AdNDP thus recovers not only the classical Lewis bonding elements (lone pairs and 2c-2e bonds), but also the delocalized *n*c-2e bonds. The AdNDP results for **1** correctly recover the triple bonds in the two terminal boronyl groups (B3—O5 and B2—O6; see Fig. 2(a) for the labels of atoms), the three single bonds associated with the central B atom (B4—B3, B4—B2, and B4—O8), and the 3c-1e BBB bond. In terms of the bonding within the OBO unit, the AdNDP results clearly recover the B1—O7 triple bond, consistent with its short distance.

The bond order between B1 and O8 in **1** is somewhat puzzling: AdNDP indeed reveals two B1—O8 π bonds. However, it also suggests a B1 and O8 σ bond (Fig. 3(a), the second row). The collective "triple" bond between B1 and O8 is inconsistent with the corresponding bond distance (1.29 Å; Fig. 2(a)). The BO triple bond is relatively rigid with typical distances of 1.21–1.24 Å.[79] To resolve this issue, it is essential to trace back the B1—O8 σ "bond" to the CMO. The corresponding CMO is in fact based on the O 2s atomic orbital (AO) from the O8 atom (88%), nearly identical to the O 2s lone-pairs on the O5, O6, and O7 atoms (88%, 91%, and 93%, respectively). Thus, B1—O8 σ "bond" is equivalent to an O 2s lone-pair and the B1—O8 bond should be viewed as double bond.

For an in-depth understanding of the bonding nature of the OBO unit in **1**, we plotted the corresponding CMOs in Fig. 4(a). Five CMOs are primarily responsible for the OBO bonding; HOMO–14 (Fig. 4(b)) may contribute slightly to the B1—O8 σ bonding, but it is primarily responsible for the B4—O8 single bond (see below for its Wiberg bond index). HOMO–10 is the B1—O7 σ bond. The combination of O $2p_z$ AOs results in HOMO–2 and HOMO–11. The former is essentially nonbonding with 61% and 15% O $2p_z$ contribution from the two O centers, while the latter is a completely bonding π CMO. Thus, HOMO–2 and HOMO–11 form a 3c–4e π hyperbond, which is reminiscent of the prototypical 3c-4e σ hyperbond (ω-bond) in XeF_2 or FHF^-.[80] The

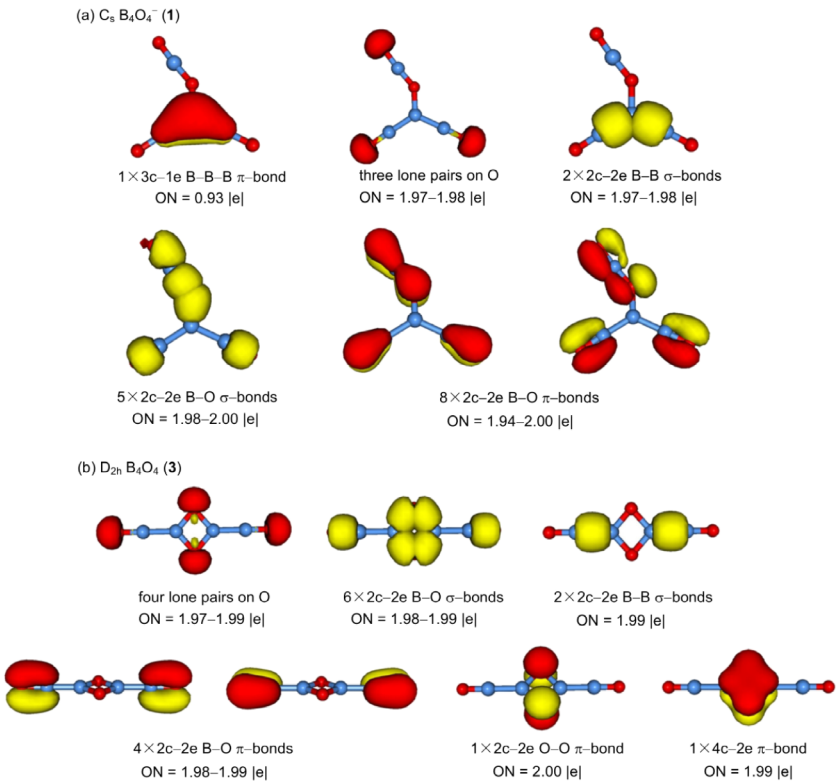

FIG. 3. AdNDP bonding patterns for (a) $B_4O_4^-$ (**1**, C_s) and (b) B_4O_4 (**3**, D_{2h}). The occupation numbers (ONs) are shown. See text for discussion of the nature of the B—O σ "bond" between B1 and O8 in **1** (atom labels as shown in Fig. 2(a)), which can be traced back to the CMO as an O 2s lone pair.

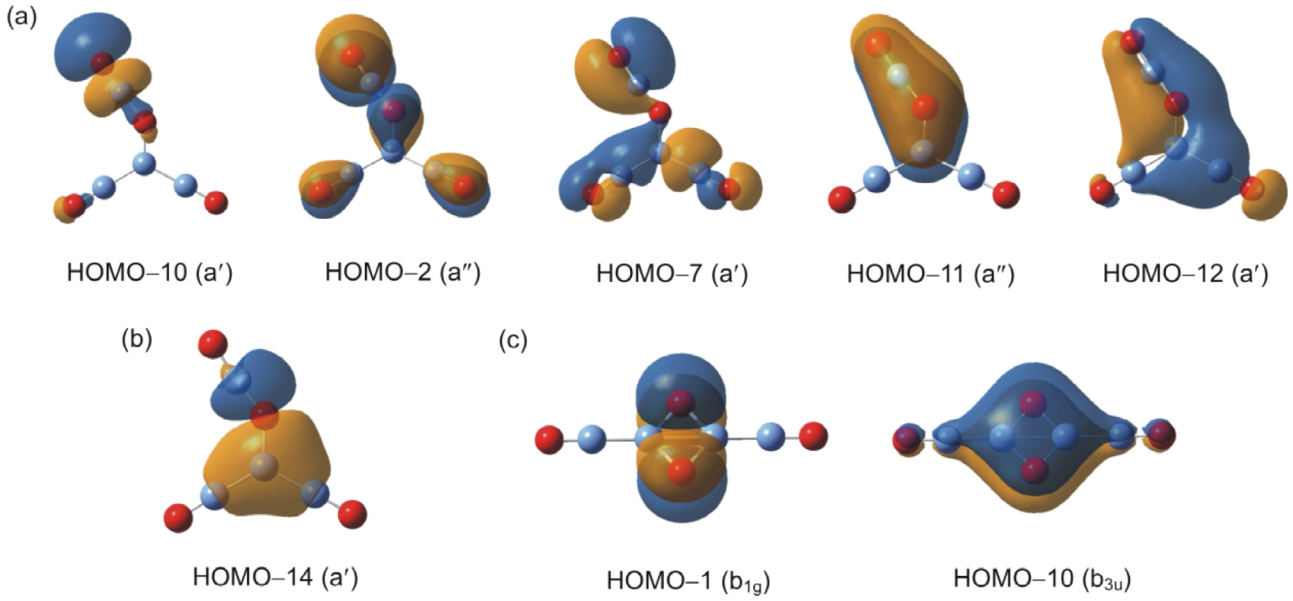

FIG. 4. Key bonding elements as revealed from the CMO analyses: (a) dual 3c–4e hypervalent π bonds in $B_4O_4^-$ (**1**). (b) The B—O single bond in $B_4O_4^-$ (**1**). (c) Rhombic 4c–4e π bond (*o*-bond) in $B_4O_4^-$ (**2**).

difference is that the current 3c–4e hyperbond is a π bond in the p_z manifold, while that in XeF_2 and FHF^- is a σ bond. Similarly, the bonding/nonbonding combination of HOMO–7 and HOMO–12 forms a 3c–4e π hyperbondin the p_y manifold: HOMO–7 is largely contributed from the O7 (46%) and HOMO–12 is completely bonding. Although the four π CMOs in OBO have severely unbalanced O contributions, their analogy to the 3c-4e σ hyperbond in XeF_2 or FHF^- suggests that the bonding nature of the OBO unit should be described as dual 3c-4e π hyperbonds. The dual 3c-4e π hyperbonds in combination with the B1—O7 σ bond collectively generate the triple B1≡O7 and double B1═O8 bonds, in line with their bond distances. On the basis of the above analysis, the approximate Lewis presentation of **1** is illustrated in Fig. 5(a).[81]

The NBO analysis helps to shed further light on the difference between the B1≡O7, B1═O8, and B4—O8 bonds in **1**. It is known that, due to the polar nature of the BO bonding, the Wiberg bond index for the B≡O triple bond is always lower than 3.0.[46–52,55,56] However, the Wiberg bond indices indeed differ markedly for the B1≡O7, B1═O8, and B4—O8 bonds, which are 1.69, 1.05, and 0.71, respectively, correlating well with their formal bond orders. For comparison, the Wiberg bond indices for the boronyl groups in **1** are 1.75/1.76.

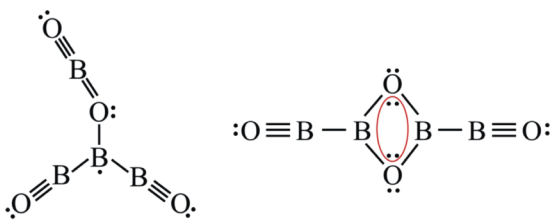

FIG. 5. Schematic Lewis presentation of the global-minimum structures in different charge states: (a) $B_4O_4^-$ (**1**, C_s) and (b) B_4O_4 (**3**, D_{2h}).

C. The rhombic D_{2h} structures 2 and 3: The *o*-bond

Very recently, the concept of *o*-bond, that is, rhombic 4c-4e π bond, was proposed in boron oxide clusters.[55] An *o*-bond involves a delocalized, bonding CMO along with an essentially nonbonding one, in a rhombic B_2O_2 structural motif. Here, we report the first experimental characterization of such species in the gas phase. The minor isomer (X′; Fig. 1) in the experimental PES spectra of $B_4O_4^-$ is structure **2**, whose corresponding neutral species **3** is the global minimum at this charge state. Structure **3** is reached from **2** in the present experiment upon photodetachment. A rhombic B_2O_2 unit forms the core of **2** and **3**, terminated by two boronyl groups (Fig. 2). The bonding of **2** and **3** are relatively straightforward. The AdNDP results of **3** are shown in Fig. 3(b): the four O 2s lone-pairs, two terminal B≡O triple bonds, two B—B single bonds, and four rhombic B—O single bonds are all recovered.

The remaining two bonds in **3** are responsible for the global bonding in the rhombic B_2O_2 ring: the 2c-2e O—O π bond and the 4c-2e π bond (Fig. 3(b), the second row). The latter bond is delocalized, and the former is again essentially nonbonding. The two corresponding CMOs are shown in Fig. 4(c), which are similar to the above AdNDP results. Here, HOMO–10 is primarily composed of O $2p_z$ and B $2p_z$ AOs in the B_2O_2 ring, forming a delocalized and completely bonding π orbital, whereas HOMO–1 is nonbonding due to pure O $2p_z$ AOs (50% O6 versus 50% O7). Thus, HOMO–10 and HOMO–1 also form a bonding/nonbonding combination. Such a rhombic 4c-4e π bond was lately described theoretically as an "*o*-bond,"[55] which is an extension of 3c-4e ω bond from three-center to four-center systems. The approximate Lewis structure for **3** is shown in Fig. 5(b).[81]

To our knowledge, the **2** and **3** species represent the first experimentally characterized molecular system with an *o*-bond. A 4c-4e *o*-bond takes advantage of the electron delocalization in the ring and makes use of two O 2p lone-pairs for a delocalized, completely bonding π CMO and a "residual"

nonbonding π CMO, which effectively stabilizes such an electron-deficient system.

VII. CONCLUSIONS

Boron oxide clusters and boronyl clusters are an emerging and expanding field in boron chemistry.[82] In this paper, we report a joint experimenal and theoretical study on the $B_4O_4^{0/-}$ clusters, each including the Y-shaped C_s and rhombic D_{2h} isomers (**1**–**4**). Both C_s (**1**) and D_{2h} (**2**) anion isomers are observed in the experimental cluster beam, with the C_s global-minimum structure being predominant. The neutral C_s (**4**) and D_{2h} (**3**) isomers are reached upon photodetachment, which possess markedly different electron affinities: 1.42 eV for D_{2h} versus 2.64 eV for C_s. Chemical bonding analyses reveal the dual 3c-4e ω hyperbonds in **1** and **4** and the rhombic 4c-4e *o*-bond in **2** and **3**. This work represents the first experimental study of a molecular system with an *o*-bond.

ACKNOWLEDGMENTS

This work was supported by the National Natural Science Foundation of China (21243004, 21373130, and 21273246), the Shanxi International Cooperation project (No. 2013081 018), and the State Key Laboratory of Quantum Optics and Quantum Optics Devices (KF201402). H.J.Z. gratefully acknowledges the start-up fund from Shanxi University for support.

[1]H. J. Zhai, L. S. Wang, A. N. Alexandrova, and A. I. Boldyrev, J. Phys. Chem. A **107**, 9319 (2003).
[2]H. J. Zhai, L. S. Wang, A. N. Alexandrova, and A. I. Boldyrev, J. Chem. Phys. **117**, 7917 (2002).
[3]A. N. Alexandrova, A. I. Boldyrev, H. J. Zhai, L. S. Wang, E. Steiner, and P. W. Fowler, J. Phys. Chem. A **107**, 1359 (2003).
[4]A. N. Alexandrova, A. I. Boldyrev, H. J. Zhai, and L. S. Wang, J. Phys. Chem. A **108**, 3509 (2004).
[5]H. J. Zhai, A. N. Alexandrova, K. A. Birch, A. I. Boldyrev, and L. S. Wang, Angew. Chem., Int. Ed. **42**, 6004 (2003).
[6]A. N. Alexandrova, H. J. Zhai, L. S. Wang, and A. I. Boldyrev, Inorg. Chem. **43**, 3552 (2004).
[7]H. J. Zhai, B. Kiran, J. Li, and L. S. Wang, Nat. Mater. **2**, 827 (2003).
[8]A. P. Sergeeva, D. Y. Zubarev, H. J. Zhai, A. I. Boldyrev, and L. S. Wang, J. Am. Chem. Soc. **130**, 7244 (2008).
[9]A. N. Alexandrova, A. I. Boldyrev, H. J. Zhai, and L. S. Wang, J. Chem. Phys. **122**, 054313 (2005).
[10]C. Romanescu, D. J. Harding, A. Fielicke, and L. S. Wang, J. Chem. Phys. **137**, 014317 (2012).
[11]W. Huang, A. P. Sergeeva, H. J. Zhai, B. B. Averkiev, L. S. Wang, and A. I. Boldyrev, Nat. Chem. **2**, 202 (2010).
[12]B. Kiran, S. Bulusu, H. J. Zhai, S. Yoo, X. C. Zeng, and L. S. Wang, Proc. Natl. Acad. Sci. U. S. A. **102**, 961 (2005).
[13]A. N. Alexandrova, A. I. Boldyrev, H. J. Zhai, and L. S. Wang, Coord. Chem. Rev. **250**, 2811 (2006).
[14]Z. A. Piazza, W. L. Li, C. Romanescu, A. P. Sergeeva, L. S. Wang, and A. I. Boldyrev, J. Chem. Phys. **136**, 104310 (2012).
[15]A. P. Sergeeva, Z. A. Piazza, C. Romanescu, W. L. Li, A. I. Boldyrev, and L. S. Wang, J. Am. Chem. Soc. **134**, 18065 (2012).
[16]I. A. Popov, Z. A. Piazza, W. L. Li, L. S. Wang, and A. I. Boldyrev, J. Chem. Phys. **139**, 144307 (2013).
[17]Z. A. Piazza, I. A. Popov, W. L. Li, R. Pal, X. C. Zeng, A. I. Boldyrev, and L. S. Wang, J. Chem. Phys. **141**, 034303 (2014).
[18]W. L. Li, Y. F. Zhao, H. S. Hu, J. Li, and L. S. Wang, Angew. Chem., Int. Ed. **53**, 5540 (2014).
[19]W. L. Li, Q. Chen, W. J. Tian, H. Bai, Y. F. Zhao, H. S. Hu, J. Li, H. J. Zhai, S. D. Li, and L. S. Wang, J. Am. Chem. Soc. **136**, 12257 (2014).
[20]Z. A. Piazza, H. S. Hu, W. L. Li, Y. F. Zhao, J. Li, and L. S. Wang, Nat. Commun. **5**, 3113 (2014).
[21]Q. Chen, G. F. Wei, W. J. Tian, H. Bai, Z. P. Liu, H. J. Zhai, and S. D. Li, Phys. Chem. Chem. Phys. **16**, 18282 (2014).
[22]B. C. Hikmat, T. Baruah, and R. R. Zope, J. Phys. B: At., Mol. Opt. Phys. **45**, 225101 (2012).
[23]H. T. Pham, L. V. Duong, B. Q. Pham, and M. T. Nguyen, Chem. Phys. Lett. **577**, 32 (2013).
[24]S. Chacko, D. G. Kanhere, and I. Boustani, Phys. Rev. B **68**, 035414 (2003).
[25]I. Boustani, A. Rubio, and J. A. Alonso, Chem. Phys. Lett. **311**, 21 (1999).
[26]I. Boustani, A. Quandt, and A. Rubio, J. Solid State Chem. **154**, 269 (2000).
[27]F. Y. Tian and Y. X. Wang, J. Chem. Phys. **129**, 024903 (2008).
[28]H. T. Pham, L. V. Duong, N. M. Tam, M. P. Pham-Ho, and M. T. Nguyen, Chem. Phys. Lett. **608**, 295 (2014).
[29]W. L. Li, C. Romanescu, T. Jian, and L. S. Wang, J. Am. Chem. Soc. **134**, 13228 (2012).
[30]D. Z. Li, Q. Chen, Y. B. Wu, H. G. Lu, and S. D. Li, Phys. Chem. Chem. Phys. **14**, 14769 (2012).
[31]H. Bai, Q. Chen, C. Q. Miao, Y. W. Mu, Y. B. Wu, H. G. Lu, H. J. Zhai, and S. D. Li, Phys. Chem. Chem. Phys. **15**, 18872 (2013).
[32]H. J. Zhai, Q. Chen, H. Bai, H. G. Lu, W. L. Li, S. D. Li, and L. S. Wang, J. Chem. Phys. **139**, 174301 (2013).
[33]H. J. Zhai, Y. F. Zhao, W. L. Li, Q. Chen, H. Bai, H. S. Hu, Z. A. Piazza, W. J. Tian, H. G. Lu, Y. B. Wu, Y. W. Mu, G. F. Wei, Z. P. Liu, J. Li, S. D. Li, and L. S. Wang, Nat. Chem. **6**, 727 (2014).
[34]H. Bai, Q. Chen, H. J. Zhai, and S. D. Li, Angew. Chem., Int. Ed. **54**, 941 (2015).
[35]Q. Chen, W. L. Li, Y. F. Zhao, S. Y. Zhang, H. S. Hu, H. Bai, H. R. Li, W. J. Tian, H. G. Lu, H. J. Zhai, S. D. Li, J. Li, and L. S. Wang, ACS Nano **9**, 754 (2015).
[36]H. C. Longuet-Higgins, J. Chim. Phys. **46**, 268 (1949).
[37]L. Hanley and S. L. Anderson, J. Chem. Phys. **89**, 2848 (1988).
[38]D. Peiris, A. Lapicki, S. L. Anderson, R. Napora, D. Linder, and M. Page, J. Phys. Chem. A **101**, 9935 (1997).
[39]T. R. Burkholder and L. Andrews, J. Chem. Phys. **95**, 8697 (1991).
[40]M. L. Drummond, V. Meunier, and B. G. Sumpter, J. Phys. Chem. A **111**, 6539 (2007).
[41]X. J. Feng, Y. H. Luo, X. Liang, L. X. Zhao, and T. T. Cao, J. Cluster Sci. **19**, 421 (2008).
[42]T. B. Tai and M. T. Nguyen, Chem. Phys. Lett. **483**, 35 (2009).
[43]M. T. Nguyen, M. H. Matus, V. T. Ngan, D. J. Grant, and D. A. Dixon, J. Phys. Chem. A **113**, 4895 (2009).
[44]T. B. Tai, M. T. Nguyen, and D. A. Dixon, J. Phys. Chem. A **114**, 2893 (2010).
[45]C. B. Shao, L. Jin, and Y. H. Ding, J. Comput. Chem. **32**, 771 (2011).
[46]H. J. Zhai, S. D. Li, and L. S. Wang, J. Am. Chem. Soc. **129**, 9254 (2007).
[47]S. D. Li, H. J. Zhai, and L. S. Wang, J. Am. Chem. Soc. **130**, 2573 (2008).
[48]H. J. Zhai, J. C. Guo, S. D. Li, and L. S. Wang, ChemPhysChem **12**, 2549 (2011).
[49]H. J. Zhai, C. Q. Miao, S. D. Li, and L. S. Wang, J. Phys. Chem. A **114**, 12155 (2010).
[50]H. Bai, H. J. Zhai, S. D. Li, and L. S. Wang, Phys. Chem. Chem. Phys. **15**, 9646 (2013).
[51]Q. Chen, H. J. Zhai, S. D. Li, and L. S. Wang, J. Chem. Phys. **137**, 044307 (2012).
[52]W. Z. Yao, J. C. Guo, H. G. Lu, and S. D. Li, J. Phys. Chem. A **113**, 2561 (2009).
[53]R. J. Doyle, J. Am. Chem. Soc. **110**, 4120 (1988).
[54]H. Braunschweig, K. Radacki, and A. Schneider, Science **328**, 345 (2010).
[55]Q. Chen, H. G. Lu, H. J. Zhai, and S. D. Li, Phys. Chem. Chem. Phys. **16**, 7274 (2014).
[56]W. J. Tian, H. G. Xu, X. Y. Kong, Q. Chen, W. J. Zheng, H. J. Zhai, and S. D. Li, Phys. Chem. Chem. Phys. **16**, 5129 (2014).
[57]D. Z. Li, H. Bai, Q. Chen, H. G. Lu, H. J. Zhai, and S. D. Li, J. Chem. Phys. **138**, 244304 (2013).
[58]H. G. Xu, Z. G. Zhang, Y. Feng, J. Y. Yuan, Y. C. Zhao, and W. J. Zheng, Chem. Phys. Lett. **487**, 204 (2010).
[59]A. P. Sergeeva, B. B. Averkiev, H. J. Zhai, A. I. Boldyrev, and L. S. Wang, J. Chem. Phys. **134**, 224304 (2011).
[60]M. Saunders, J. Comput. Chem. **25**, 621 (2004).
[61]S. De, A. Willand, M. Amsler, P. Pochet, L. Genovese, and S. Goedecker, Phys. Rev. Lett. **106**, 225502 (2011).
[62]S. Goedecker, J. Chem. Phys. **120**, 9911 (2004).
[63]S. Goedecker, W. Hellmann, and T. Lenosky, Phys. Rev. Lett. **95**, 055501 (2005).

[64]R. A. Kendall, T. H. Dunning, and R. J. Harrison, J. Chem. Phys. **96**, 6796 (1992).
[65]M. E. Casida, C. Jamorski, K. C. Casida, and D. R. Salahub, J. Chem. Phys. **108**, 4439 (1998).
[66]R. Bauernschmitt and R. Ahlrichs, Chem. Phys. Lett. **256**, 454 (1996).
[67]W. von Niessen, J. Schirmer, and L. S. Cederbaum, Comput. Phys. Rep. **1**, 57 (1984).
[68]V. G. Zakrzewski and J. V. Ortiz, Int. J. Quantum Chem. **53**, 583 (1995).
[69]J. V. Ortiz, Adv. Quantum Chem. **35**, 33 (1999).
[70]J. Cizek, Adv. Chem. Phys. **14**, 35 (1969).
[71]G. E. Scuseria and H. F. Schaefer, J. Chem. Phys. **90**, 3700 (1989).
[72]R. J. Bartlett and M. Musial, Rev. Mod. Phys. **79**, 291 (2007).
[73]D. Y. Zubarev and A. I. Boldyrev, Phys. Chem. Chem. Phys. **10**, 5207 (2008).
[74]E. D. Glendening, J. K. Badenhoop, A. E. Reed, J. E. Carpenter, J. A. Bohmann, C. M. Morales, and F. Weinhold, *NBO 5.0* (Theoretical Chemistry Institute, University of Wisconsin, Madison, 2001).
[75]M. J. Frisch *et al.*, GAUSSIAN 09, Revision D.01, Gaussian, Inc. Wallingford, CT, 2009.
[76]See supplementary material at http://dx.doi.org/10.1063/1.4916386 for optimized coordinates for C_s $B_4O_4^-$ (**1**), D_{2h} $B_4O_4^-$ (**2**), D_{2h} B_4O_4 (**3**), and C_s B_4O_4 (**4**) at the B3LYP/aug-cc-pVTZ level; low-lying isomers of $B_4O_4^{0/-}$ at the B3LYP/aug-cc-pVTZ level; energy levels of the frontier canonical molecular orbitals (CMOs) of $B_4O_4^-$ (**1**, C_s) and $B_4O_4^-$ (**2**, D_{2h}); and natural charge distribution of the global minima and relevant structures for $B_4O_4^{0/-}$.
[77]A. Moezzi, R. A. Bartlett, and P. P. Power, Angew. Chem., Int. Ed. Engl. **31**, 1082 (1992).
[78]A. Moezzi, M. M. Olmstead, and P. P. Power, J. Am. Chem. Soc. **114**, 2715 (1992).
[79]P. Pyykkö and M. Atsumi, Chem.–Eur. J. **15**, 12770 (2009).
[80]F. Weinhold and C. R. Landis, *Valency and Bonding: A Natural Bond Orbital Donor-Acceptor Perspective* (Cambridge University Press, Cambridge, 2005), p. 275.
[81]Note that in Fig. 5, each B≡O triple or B=O double bond in $B_4O_4^-$ (**1**, C_s) and (b) B_4O_4 (**3**, D_{2h}) contains one dative bond, to which the O atom contributes two valence electrons solely. In the presentation, each B atom is illustrated explicitly for three valence electrons, and each O atom for six. Thus, none of the B atoms in **1** and **3** goes beyond trivalency, as anticipated.
[82]H. J. Zhai, Q. Chen, H. Bai, S. D. Li, and L. S. Wang, Acc. Chem. Res. **47**, 2435 (2014).